Temperature-Dependent Transient Absorption Spectroscopy Elucidates Trapped-Hole Dynamics in CdS and CdSe Nanorods

James Utterback, Jesse Ruzicka, Hayden Hamby, Joel Eaves, Gordana Dukovic

Temperature-Dependent Transient Absorption Spectroscopy Elucidates Trapped-Hole Dynamics in CdS and CdSe Nanorods

*James K. Utterback, Jesse L. Ruzicka, Hayden Hamby, Joel D. Eaves, Gordana Dukovic**
Department of Chemistry, University of Colorado Boulder, Boulder, Colorado 80309, USA

Corresponding Author
* E-mail: gordana.dukovic@colorado.edu

ABSTRACT

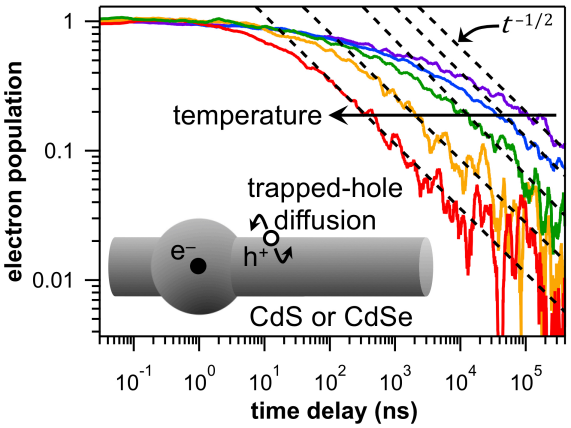

Charge-carrier traps play a central role in the excited-state dynamics of semiconductor nanocrystals, but their influence is often difficult to measure directly. In CdS and CdSe nanorods of nonuniform width, spatially-separated electrons and trapped holes display recombination dynamics that follow a power-law function in time that is consistent with trapped-hole diffusion-limited recombination. However, power-law relaxation can originate from mechanisms other than diffusion. We report transient absorption spectroscopy measurements on CdS and CdSe nanorods recorded at temperatures ranging from 160 to 294 K. We find that the exponent of the power law is temperature-independent, which rules out several models based on stochastic activated processes and provides insights into the mechanism of diffusion-limited recombination in these structures. The data point to weak electronic coupling between trap states and that surface-localized trapped holes couple strongly to phonons, leading to slow diffusion. Trap-to-trap hole hopping behaves classically near room temperature while quantum aspects of phonon-assisted tunneling become observable at low temperatures.

MAIN TEXT

Although colloidal semiconductor nanocrystals have been widely studied for three decades,[1,2] the understanding of their excited-state dynamics continues to evolve. The presence of charge-carrier trap states on nanocrystal surfaces leads to rich and complex excited-state relaxation.[3-13] Trap states play an essential role in processes such as electron–hole recombination and charge transfer,[4,6,7,14-16] yet their dynamics are challenging to probe spectroscopically.[17,18] Photogenerated holes in CdS and CdSe nanocrystals trap to the orbitals of undercoordinated S and Se atoms on the particle surface on a picosecond timescale.[3,8,17-21] Thus, electrons in these structures recombine primarily with holes that are localized to the surface, rather than delocalized in the valence band.[17,18]

We recently presented evidence that trapped holes on the surfaces of CdS and CdSe nanocrystals are not stationary but instead undergo a diffusive random walk at room temperature.[10-13,16] This evidence came from transient absorption (TA) spectroscopy measurements of recombination dynamics between spatially separated electrons and trapped holes in nonuniform CdS and CdSe nanorods (NRs). At long times, the TA signal associated with this recombination follows a robust and reproducible power law in time with an exponent of –1/2. We interpreted this behavior as the signature of diffusion-limited recombination in one dimension, where a trapped hole undergoes an unbiased random walk along the NR surface, with steps on the order of interatomic distances, until it reaches the electron and recombines.[10] Subsequent theoretical work used detailed electronic structure calculations to characterize the surface traps in CdS and found that, near room temperature, the trapped holes hop nonadiabatically between localized sulfur orbitals on the surface.[13]

There are, however, other mechanisms that can lead to power-law excited-state relaxation in nanocrystals. In particular, to model nonexponential relaxation dynamics in nanocrystals, researchers have often invoked stochastic rate theories, where there is a distribution of relaxation rates in the ensemble. Examples include electron trapping with a distribution in activation barrier heights[22] and charge-carrier detrapping with a distribution in trap depths.[23-25] An experimental method is needed to differentiate between these mechanisms and diffusion-limited recombination in nonuniform NRs.

The key measurable difference between the trapped-hole diffusion model and the alternative models listed above lies in the temperature dependence of the power-law exponent. In the one-dimensional diffusion–annihilation model, the temperature dependence appears in the magnitude of the diffusion coefficient while the power-law exponent of –1/2 is uniquely determined by the geometry.[26] In contrast, models that involve thermally-activated processes give rise to temperature-dependent power-law exponents.[22,25] In this paper we present TA spectroscopy of solutions of CdS and CdSe NRs over a range of temperatures from 160 to 294 K. From these data, we extract the temperature dependence of the power-law exponent and provide an experimental method to definitively distinguish between diffusion-limited recombination and stochastic rate theories. In concert with the diffusion-limited recombination theory, these experiments inform on the mechanism of the diffusion process, providing measurements of both the electronic coupling between hole trap states and the trapped hole–phonon coupling. At high temperatures and weak electronic coupling, the reorganization energy alone quantifies the strength of the hole-phonon coupling.

Prior evidence for trapped-hole diffusion comes from TA spectroscopy of nonuniform nanorods of CdS and CdSe at room temperature.[10-12] Such NRs consist of narrow-diameter cylindrical “rods” and wide-diameter “bulbs” (Figure 1a,b and Figure S1).[10,12,27,28] The rod and bulb morphological features constitute spatially and spectrally distinct electronic states wherein charge carriers in the rod have higher energy than in the bulb due to differences in radial quantum confinement (Figure 1c).[10,12,28] As described previously in room-temperature TA studies,[10-12] trapped holes likely diffuse in nanostructures of uniform morphologies as well, but the spatial dynamics of trapped holes are revealed in these nonuniform NRs when holes rapidly trap on the rod surface and electrons dissociate from them and localize in the bulb so that recombination can only occur if the electron and trapped hole reach each other in some way.

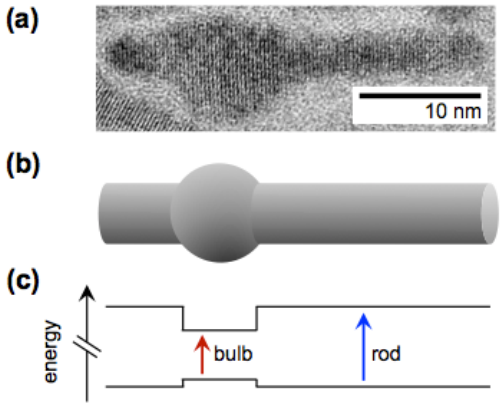

Figure 1. Morphology and energy-level diagram for nonuniform nanorods. (a) Selected transmission electron microscope image of a nonuniform CdS nanorod. (b) Schematic diagram of a nonuniform nanorod, depicting the rod and bulb components. (c) Energy-level diagram as a function of position along the nanorod, according to (b).

To carry out TA spectroscopy measurements at cryogenic temperatures, the NRs were functionalized with 3-mercaptopropanoic acid surface-capping ligands and suspended in a polar glass-forming mixture of 4:1 ethanol:methanol (v/v). Temperature was controlled using a cryostat purged with a nitrogen atmosphere, and experiments were limited to temperatures above the glass-transition temperature of the solution. Figure 2a,b show the TA spectra of CdS and CdSe NRs after excitation of the rod at temperatures ranging from 160 to 294 K. As temperature decreases, the bleach peaks shift to higher energies and become narrower, as is observed in bulk and nanocrystalline semiconductors (Figure S2).[29,30] The TA spectrum of nonuniform nanorods consists of distinct spectral features corresponding to the rod and the bulb states (Figure 2), the amplitudes of which predominantly reflect the population of electrons in each state.[10,12,27,28,31] The dynamics of electrons in the rod and bulb states were isolated and analyzed as described previously for room-temperature experiments (see Methods section and Section IV of the Supporting Information (SI)).[10,12] The data shown in Figure S3 indicate that sub-nanosecond spatial separation occurs at each temperature, leading to a charge-separated state where the electron is localized in the bulb and the hole is trapped on the surface of the rod (Figure 2c,d inset).

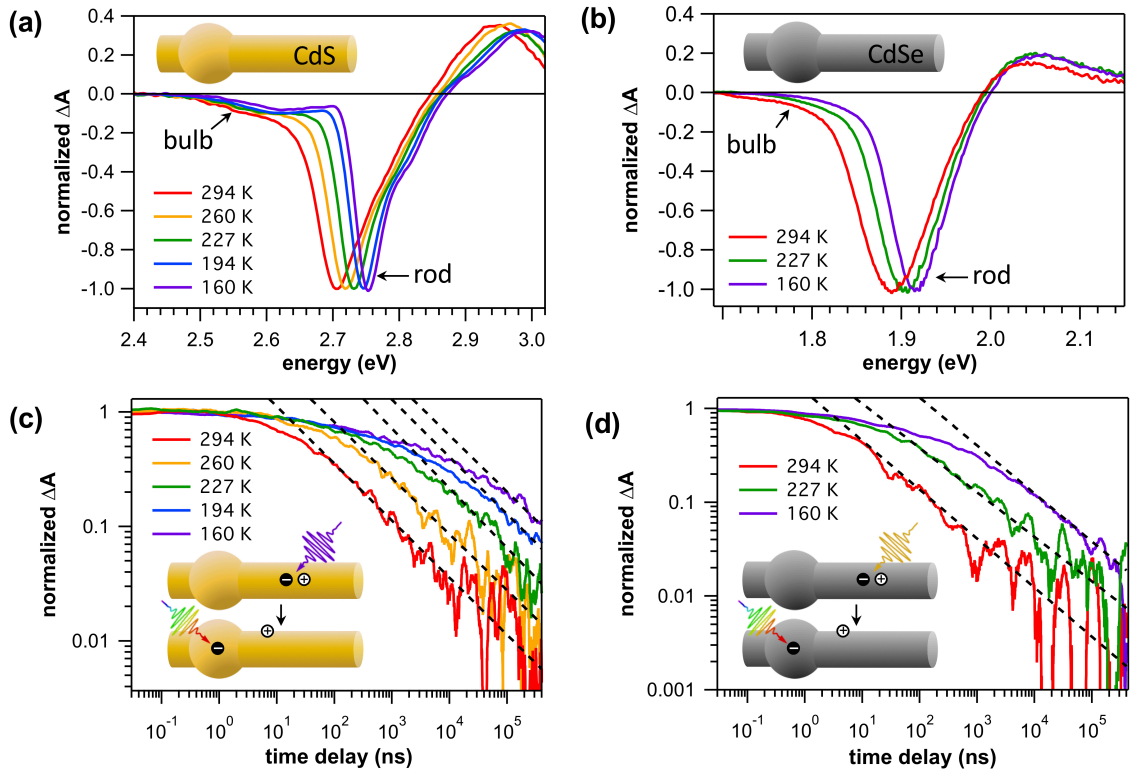

Figure 2. Temperature dependence of excited-state dynamics in CdS and CdSe nanorods. (a,b) Normalized TA spectra at different temperatures between 160 and 294 K of (a) CdS NRs averaged over 100–300 ns and (b) CdSe NRs averaged over 1–3 ns. CdS NRs were excited with 400 nm pulses and CdSe NRs were excited with 600 nm pulses. The parts of the bleach assigned to bulb and rod transitions are marked with arrows. (c,d) TA time traces of bulb bleach signal of (c) CdS NRs and (d) CdSe NRs normalized at 100 ps. Power-law tails were fit with an adjustable power-law exponent (black dashed lines). Data are smoothed for presentation. The insets of (c,d) depict the charge-separated state being probed after excitation of the rod.

To investigate the recombination dynamics of spatially separated electrons and trapped holes in CdS and CdSe NRs as a function of temperature, we monitor the decay of the TA bleach signal corresponding to the bulb electron population in the time window after charge separation at temperatures ranging from 160 to 294 K. Bulb decays for CdS NRs at five different temperatures are shown in Figure 2c, while the equivalent data for CdSe NRs at three different temperatures are shown in Figure 2d. At 294 K, both materials exhibit power-law decays at long times, consistent with previous observations.[10,12] As the temperature is lowered, the bulb electron relaxation gets slower but the power-law decay persists at every temperature. This is in contrast to the recombination kinetics in uniform NRs, which exhibit exponential tails at all temperatures in the range 160 to 294 K (Figure S4) due to direct recombination of spatially overlapping electrons and trapped holes.[10,12]

As we noted above, the temperature dependence of the exponent in a power-law decay can provide definitive insights into the mechanism of electron–hole recombination that leads to the power law. The tails of each decay in Figures 2c and 2d were fit to a power-law function of the form $S(t) \sim t^{-\alpha}$ (see Methods). The fit results are plotted in Figure 3. For every temperature studied, the power-law exponent is within experimental error of –1/2 for both CdS and CdSe NRs.

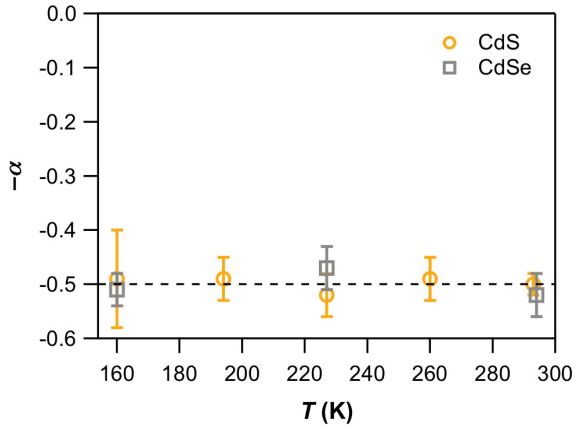

Figure 3. The extracted exponent of the power-law decay, $-\alpha$, in nonuniform CdS and CdSe NRs is independent of temperature.

The persistence of the power-law exponent of –1/2 over a broad range of temperatures in both CdS and CdSe NRs strongly supports the assignment of power-law recombination kinetics to diffusion-limited recombination between the bulb electron and a trapped hole. In this model, the trapped hole starts near the bulb and undergoes an unbiased random walk along the length of the rod until it encounters the stationary electron in the bulb and recombines with it.[10] Diffusion purely around the circumference of the rod does not contribute to decay of the bulb electron, so recombination is a one-dimensional process.[10] While temperature can change the diffusion coefficient, a power-law exponent of –1/2 is a universal feature of diffusion–annihilation in one dimension and is independent of temperature.[26]

The temperature independence of the power-law exponent allows us to rule out models in which there is a distribution in rate constants for recombination in an ensemble of particles. Power-law kinetics can arise in an ensemble of particles when their first-order rate constants reflect a thermally-activated process and there is an exponential distribution in the activation energies, $P(E_\mathrm{a}) = e^{-E_\mathrm{a}/\epsilon}/\epsilon$, where E_a is the activation energy and ϵ represents the mean barrier height, which is independent of temperature. In this case, the decay of the ensemble excited-state population goes as $S(t) \sim t^{-\alpha}$ at long times, where the power-law exponent $\alpha = k_\mathrm{B}T/\epsilon$ depends on temperature (T) as well as the material properties of the sample that determine ϵ, such as composition, size, and ligands.[22,25] There are several plausible scenarios in which the observed power-law decay of the bulb electron population could be due to such activated mechanisms. Electrons could trap from the bulb state while the trapped hole remains stationary on the rod,[10,32,33] in which case the power-law decay of the electron population would reflect a distribution in electron trapping rates,[34-36] which could originate from a distribution in trapping activation barriers.[22] Additionally, recombination could occur by thermal excitation of the electron from the bulb back to the rod where it would overlap directly with the trapped hole. In this case, a distribution of rate constants would reflect a distribution in relative rod and bulb radii. Finally, recombination could be limited by detrapping of the hole: a stationary trapped hole could eventually return to the valence band with a distribution of hole detrapping times that originates from a distribution in trap depths,[23-25] and from there it would rapidly transfer to the bulb where it would recombine with the electron.

Each of these mechanisms can be ruled out by the lack of temperature independence of the experimentally measured power-law exponent of the bulb electron decay (Figure 3). If the power-law tails observed in CdS and CdSe NRs in Figure 2 were due to an activated mechanism, α would

be proportional to temperature and would have changed by nearly a factor of two over the temperature range studied. Moreover, even though the distributed activated models could give rise to a power-law decay, one would expect α to be highly sensitive to sample preparation, because sample-to-sample variation is likely to cause significant changes in the value of ϵ in the distributions of, for example, the relative sizes of the rods and bulbs, electron trapping barriers or the hole trap depths. Not only is the power-law exponent temperature independent, it has proven to be robust and insensitive to many sample-dependent quantities. It has been measured in over twenty CdS NR samples to date, ZnSe/CdS and CdSe/CdS dot-in-rod heterostructures, and CdSe NRs.[10-12] The same exponent appears also for both native phosphonic acid ligands and mercaptocarboxylate ligands.[10] Thus, the temperature dependence data and the reproducibility of α favor a model in which the fundamental microscopic behavior is robust to sample variation and composition, depending only on a universal property of these systems, such as the dimensionality. Separately, we note that the notion of recombination via hole detrapping in our samples is inconsistent with the low photoluminescence quantum yields typically observed in CdS and CdSe nanocrystals,[4,37,38] which imply that electrons predominantly recombine with trapped holes rather than valence-band holes.[18] It is worth noting that the present work does not indicate that the above activated processes do not occur on some timescale, just that they do not dominate the mechanism behind the power-law decay of charge-separated electrons and trapped holes in CdS and CdSe NRs.

We next examine the temperature dependence of the trapped-hole hopping rate to gain insights into the nature of the trapped-hole diffusion mechanism. For a trapped hole that begins at a distance z_0 from the bulb and diffuses with diffusion coefficient D, the onset of the $t^{-1/2}$ power-law tail of the survival probability occurs on a timescale of approximately $\tau = z_0^2/4D$ (see Section VI of the SI).[10,26] The diffusion coefficient, in turn, is related to the step length of the random walk, a, and the hole-hopping rate, κ, by $D = a^2\kappa$.[13,26] For diffusion along the length of the nanorod, a is the lattice constant for the wurtzite c-axis and κ is the total hopping rate that is composed of chalcogenide-to-chalcogenide hole hopping steps that are both parallel with and diagonal to the wurtzite c-axis.[13] The extent of lattice contraction over the measured temperature range is negligible (~0.1%),[39] making a approximately constant with respect to temperature. We also assume that the initial distribution of trapped-hole positions does not change substantially with temperature. In this case, the temperature dependence of the observable τ is inversely proportional to the temperature dependence of the hole-hopping rate: $\tau^{-1}(T) = \frac{4D}{z_0^2} = \frac{4a^2}{z_0^2}\kappa(T)$. The data in Figure 2 allow us to extract the lower and upper bounds of τ, which yield bounds on the hole-hopping rates in CdS and CdSe nanorods. The procedure for extracting the bounds of τ is described in Section VI of the SI (Figure S5). Figure 4 shows the resulting range, displayed as an Arrhenius plot of τ^{-1}.

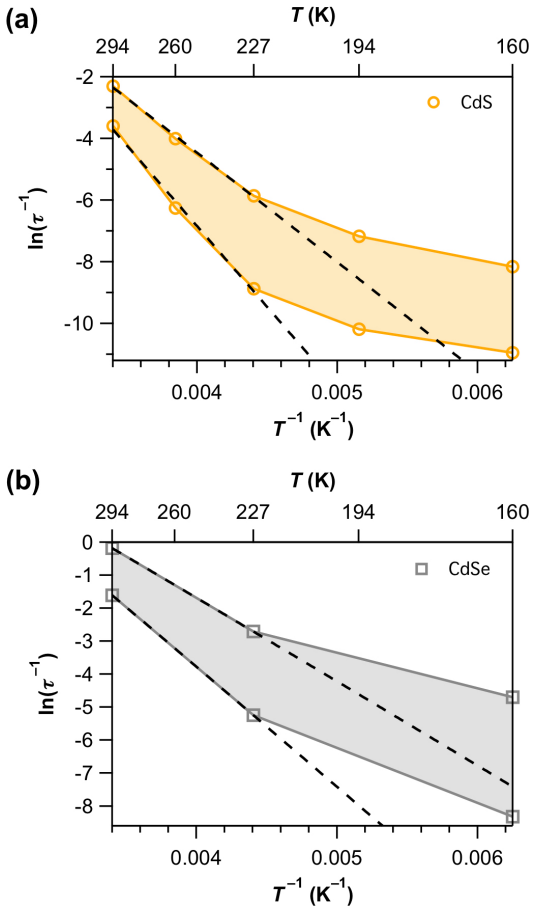

Figure 4. Arrhenius plot of hole-hopping rate in (a) CdS and (b) CdSe NRs. Data is plotted as the natural log of τ^{-1} against T^{-1}, where τ is in units of nanoseconds. Data in the range 227–294 K is fitted with the expression for classical Marcus theory (black dashed line).

At higher temperatures (227–294 K), the hole-hopping rate exhibits Arrhenius behavior (Figure 4). This result is consistent with previous theoretical calculations, which suggested that the trapped hole undergoes a series of incoherent, thermally-activated hops between trap sites on the nanocrystal surface.[13] In this mechanism, the rate of hole transfer between degenerate trap states at high temperatures is given by classical Marcus theory, $\kappa = \frac{2\pi}{\hbar}|J|^2 \frac{1}{\sqrt{4\pi\lambda k_B T}} \exp(-\lambda/4k_B T)$, where λ is the reorganization energy and $|J|^2$ is the electronic coupling between the initial and final states.[40] In this experiment we are only sensitive to trapped-hole motion along the length of the nanorod,[10] so λ and $|J|^2$ here are specifically associated with chalcogenide-to-chalcogenide hole hopping steps with a component along the wurtzite *c*-axis.[13] The data for the upper and lower bounds of $\tau^{-1}(T)$ in Figure 4 were fit to the expression for classical Marcus theory over the range of 227 to 294 K to find the upper and lower bounds of λ and $|J|^2$. The values of λ come directly from the slope of the Arrhenius plot, giving 1.2–1.9 eV and 1.0–1.4 eV for CdS and CdSe NRs, respectively. We obtain estimates for $|J|^2$ from the intercept of Figure 4 using the wurtzite *c*-axis lattice constants of CdS and CdSe[39] for a and the previous estimates for z_0, which are on the order of 1 nm for both CdS and CdSe NRs.[10,12] This gives estimates for $\sqrt{|J|^2}$ of 20–300 meV and 20–100 meV for CdS and CdSe NRs, respectively. These values for $|J|^2$ and λ in turn give estimates for D at room temperature of 10^{-9}–10^{-7} cm^2 s^{-1} and 10^{-8}–10^{-7} cm^2 s^{-1} for CdS and CdSe NRs,

respectively, and estimates for κ at room temperature of 10^6–10^7 s^{-1} and 10^7–10^8 s^{-1} for CdS and CdSe NRs, respectively. Overall, these results are consistent with theoretical predictions for weak electronic coupling between hole trap sites on nearest and next-nearest neighboring surface sulfur atoms along the length of the CdS NR.[13] The large values of λ found here are similar to calculations for diffusive carrier hopping in some polar semiconductors.[41] The small J/λ ratio indicates that the trapped holes form nonadiabatic small polarons that are highly localized on surface chalcogenide atoms and coupled strongly to phonons,[13,42] which leads to slow diffusion compared to band-edge carrier diffusion for these materials in the bulk.

At low temperatures, a fundamentally different regime of hole hopping emerges. In the range of 160 to 227 K, high-temperature classical Marcus theory breaks down and the hole-hopping rate depends more weakly on temperature (Figure 4). This behavior, together with the large estimated values of λ at higher temperatures, suggests that phonon-assisted tunneling plays an important role in trapped-hole diffusion at low temperature, and that hole hopping would be better described in the semiclassical Marcus-Jortner formulation.[43] These results are consistent with studies of trapping and detrapping in CdS and CdSe nanocrystals by low-temperature photoluminescence spectroscopy, which also suggest strong trapped carrier–phonon coupling.[6] However, quantitative modeling of trapped hole–phonon coupling using the present data is not trivial because the trapped hole may couple to a broad spectrum of bath modes made up of multiple lattice phonons and ligand vibrations.[44] Theoretical calculations are needed to map out the lattice and ligand modes that couple to trapped-hole hopping on the surfaces of CdS and CdSe nanocrystals. Our findings highlight that high-temperature Marcus theory limit may not be sufficient to understand low-temperature excited-state processes in nanocrystals.

In conclusion, this work addressed the fundamental understanding of excited-state dynamics of trapped photoexcited holes in CdS and CdSe nanocrystals. The data strongly support a model of trapped-hole diffusion, while several alternative mechanisms for power-law recombination dynamics that rely on thermally-activated decay pathways are ruled out. The temperature-dependent TA data provide quantitative insights about trapped-hole diffusion, showing that electronic coupling between neighboring trap states is weak while trapped holes couple strongly to phonons, making diffusion a slow process. Moreover, the data indicate that trap-to-trap hole hopping behaves classically at room temperature but point to a semiclassical description at low temperatures. The notion that surface-trapped holes are mobile in these nanocrystals and are governed by a semiclassical picture may provide a novel framework for the design of systems that seek to utilize trapped charge carriers for optoelectronic applications.

METHODS

Complete synthetic and experimental details appear in the Supporting Information. From measurements of the TEM images (Figure S1), we estimate that the CdS NRs studied have average rod diameters of 4.8 ± 0.4 nm, bulb diameters of 5.8 ± 0.8 nm, and lengths of 32 ± 3 nm, while for the CdSe NRs the average rod diameters are 8.1 ± 0.8 nm, the bulbs are 9.6 ± 1.2 nm, and the lengths are 39 ± 4 nm. All TA experiments were performed on nanocrystals that were functionalized with 3-mercaptopropanoic acid (3-MPA) and suspended in a glass-forming solvent mixture of 4:1 ethanol:methanol (v/v) at an optical density of ~1 at the lowest-energy absorption peak (Figure S6). The concentration of CdS and CdSe NRs used for TA experiments was about 100 nM. The sample was held in a 1 cm cryogenic cuvette equipped with a screw cap. Samples were prepared under Ar in a glovebox then immediately moved to the cryostat, which was promptly purged with nitrogen. The pump beam was passed through a depolarizer and the power

was controlled with neutral density filters. The pump beam had a beam waist of ~240 μm, pulse duration of ~150 fs, and pulse energy of 20 nJ/pulse for 400 nm excitation of the CdS NRs and 6 nJ/pulse for 600 nm excitation of the CdSe NRs. The pump powers in all cases were chosen such that the TA decay trace shapes were independent of pump power at both 294 K and 160 K so that the signal originated primarily from nanocrystals excited by a single photon.[45]

The rod and bulb decay traces were obtained by spectral averaging over the appropriate regions that isolate their signals,[10,12] accounting for the spectral shift with changing temperature. For CdS nanorods, time traces of the rod signal at 294, 260, 227, 194 and 160 K were obtained by averaging signal over the spectral windows 435–437, 434–436, 434–436, 434–436 and 433–435 nm, respectively, and the time traces of the bulb signal were obtained by averaging over 464–484, 467–476, 470–490, 478–488 and 480–490 nm, respectively. For CdSe nanorods, time traces of the rod signal at 294, 227 and 160 K were obtained by averaging signal over the spectral windows 628–629, 622–624 and 620–621 nm, respectively, and the time traces of the bulb signal were obtained by averaging signal over 665–675, 675–690 and 690–700 nm, respectively. To obtain the power-law exponents given in Figure 3, the power-law tails of the decay traces in Figure 2c,d were fit between the onset of the power law and the end of the experimental time window (400 μs). The onset of the power-law tails were determined by iteratively fitting the end of the decay to a power-law function and checking the reduced chi-squared values, progressively moving the onset to earlier times in each iteration until the reduced chi-squared values increased by 5% above the minimum value found. TA traces were smoothed using a Savitzky-Golay filter because this method preserves higher order moments of the signal.[46] Fitting was performed on raw data and the data was smoothed for presentation only.

ACKNOWLEDGMENTS

CdS nanorod synthesis was supported by the U.S. Department of Energy, Office of Science, Office of Basic Energy Sciences, Division of Chemical Sciences, Geosciences and Biosciences, through the National Renewable Energy Laboratory under Contract No. DE-AC36-08GO28308. CdSe nanorod synthesis was supported by the U.S. Department of Energy, Office of Basic Energy Sciences, Division of Materials Sciences and Engineering under Award No. DE-SC0010334. TA spectroscopy, data analysis, and modeling were supported by the Air Force Office of Scientific Research under AFOSR Award No. FA9550-15-1-0253 and the National Science Foundation Graduate Research Fellowship under Grant No. DGE 1144083 (J. K. U.). J. D. E. acknowledges support from the National Science Foundation under grant No. CHE-1455365. We thank Niels Damrauer for loan of the cryostat and Ryan Dill for assistance in its use.

REFERENCES

1. Ekimov, A. I.; Onushchenko, A. A., Quantum size effect in three-dimensional microscopic semiconductor crystals. *J. Exp. Theor. Phys. Lett.,* **1981,** *34*, 345-349.
2. Choi, C. L.; Alivisatos, A. P., From artificial atoms to nanocrystal molecules: Preparation and properties of more complex nanostructures. *Annu. Rev. Phys. Chem.,* **2010,** *61*, 369-389.
3. Klimov, V. I.; Schwarz, C. J.; McBranch, D. W.; Leatherdale, C. A.; Bawendi, M. G., Ultrafast dynamics of inter- and intraband transitions in semiconductor nanocrystals: Implications for quantum-dot lasers. *Phys. Rev. B,* **1999,** *60*, R2177-R2180.
4. Jones, M.; Scholes, G. D., On the use of time-resolved photoluminescence as a probe of nanocrystal photoexcitation dynamics. *J. Mater. Chem.,* **2010,** *20*, 3533-3538.

5. Knowles, K. E.; McArthur, E. A.; Weiss, E. A., A multi-timescale map of radiative and nonradiative decay pathways for excitons in CdSe quantum dots. *ACS Nano,* **2011,** *5*, 2026-2035.
6. Mooney, J.; Krause, M. M.; Saari, J. I.; Kambhampati, P., A microscopic picture of surface charge trapping in semiconductor nanocrystals. *J. Chem. Phys.,* **2013,** *138*, 204705.
7. McBride, J. R.; Pennycook, T. J.; Pennycook, S. J.; Rosenthal, S. J., The possibility and implications of dynamic nanoparticle surfaces. *ACS Nano,* **2013,** *7*, 8358-8365.
8. Peterson, M. D.; Cass, L. C.; Harris, R. D.; Edme, K.; Sung, K.; Weiss, E. A., The role of ligands in determining the exciton relaxation dynamics in semiconductor quantum dots. *Annu. Rev. Phys. Chem.,* **2014,** *65*, 317-339.
9. Krause, M. M.; Kambhampati, P., Linking surface chemistry to optical properties of semiconductor nanocrystalsl. *Phys. Chem. Chem. Phys.,* **2015,** *17*, 18882-18894.
10. Utterback, J. K.; Grennell, A. N.; Wilker, M. B.; Pearce, O.; Eaves, J. D.; Dukovic, G., Observation of trapped-hole diffusion on the surfaces of CdS nanorods. *Nat. Chem.,* **2016,** *8*, 1061-1066.
11. Grennell, A. N.; Utterback, J. K.; Pearce, O. M.; Wilker, M. B.; Dukovic, G., Relationships between exciton dissociation and slow recombination within ZnSe/CdS and CdSe/CdS dot-in-rod heterostructures. *Nano Lett.,* **2017,** *17*, 3764-3774.
12. Utterback, J. K.; Hamby, H.; Pearce, O.; Eaves, J. D.; Dukovic, G., Trapped-hole diffusion in photoexcited CdSe nanorods. *J. Phys. Chem. C,* **2018,** *122*, 16974-16982.
13. Cline, R. P.; Utterback, J. K.; Strong, S. E.; Dukovic, G.; Eaves, J. D., On the nature of trapped-hole states in CdS nanocrystals and the mechanism of their diffusion. *J. Phys. Chem. Lett.,* **2018,** *9*, 3532-3537.
14. Wu, K.; Du, Y.; Tang, H.; Chen, Z.; Lian, T., Efficient extraction of trapped holes from colloidal CdS nanorods. *J. Am. Chem. Soc.,* **2015,** *137*, 10224-10230.
15. Olshansky, J. H.; Balan, A. D.; Ding, T. X.; Fu, X.; Lee, Y. V.; Alivisatos, A. P., Temperature-dependent hole transfer from photoexcited quantum dots to molecular species: Evidence for trap-mediated transfer. *ACS Nano,* **2017,** *11*, 8346-8355.
16. Li, Q. Y.; Zhao, F. J.; Qu, C.; Shang, Q. Y.; Xu, Z. H.; Yu, L.; McBride, J. R.; Lian, T. Q., Two-dimensional morphology enhances light-driven H_2 generation efficiency in CdS nanoplatelet-Pt heterostructures. *J. Am. Chem. Soc.,* **2018,** *140*, 11726-11734.
17. Wei, H. H. Y.; Evans, C. M.; Swartz, B. D.; Neukirch, A. J.; Young, J.; Prezhdo, O. V.; Krauss, T. D., Colloidal semiconductor quantum dots with tunable surface composition. *Nano Lett.,* **2012,** *12*, 4465-4471.
18. Wu, K.; Zhu, H.; Liu, Z.; Rodriguez-Cordoba, W.; Lian, T., Ultrafast charge separation and long-lived charge separated state in photocatalytic CdS-Pt nanorod heterostructures. *J. Am. Chem. Soc.,* **2012,** *134*, 10337-10340.
19. Jasieniak, J.; Mulvaney, P., From Cd-rich to Se-rich–the manipulation of CdSe nanocrystal surface stoichiometry. *J. Am. Chem. Soc.,* **2007,** *129*, 2841-2848.
20. Keene, J. D.; McBride, J. R.; Orfield, N. J.; Rosenthal, S. J., Elimination of hole-surface overlap in graded CdS_xSe_{1-x} nanocrystals revealed by ultrafast fluorescence upconversion spectroscopy. *ACS Nano,* **2014,** *8*, 10665-10673.
21. Houtepen, A. J.; Hens, Z.; Owen, J. S.; Infante, I., On the origin of surface traps in colloidal II-VI semiconductor nanocrystals. *Chem. Mater.,* **2017,** *29*, 752-761.
22. Kern, S. J.; Sahu, K.; Berg, M. A., Heterogeneity of the electron-trapping kinetics in CdSe nanoparticles. *Nano Lett.,* **2011,** *11*, 3493-3498.

23. Rabouw, F. T.; Kamp, M.; van Dijk-Moes, R. J. A.; Gamelin, D. R.; Koenderink, A. F.; Meijerink, A.; Vanmaekelbergh, D., Delayed exciton emission and its relation to blinking in CdSe quantum dots. *Nano Lett.,* **2015,** *15*, 7718-7725.
24. Rabouw, F. T.; van der Bok, J. C.; Spinicelli, P.; Mahler, B.; Nasilowski, M.; Pedetti, S.; Dubertret, B.; Vanmaekelbergh, D., Temporary charge carrier separation dominates the photoluminescence decay dynamics of colloidal CdSe nanoplatelets. *Nano Lett.,* **2016,** *16*, 2047-2053.
25. Kuno, M.; Fromm, D. P.; Hamann, H. F.; Gallagher, A.; Nesbitt, D. J., "On"/"off" fluorescence intermittency of single semiconductor quantum dots. *J. Chem. Phys.,* **2001,** *115*, 1028-1040.
26. Redner, S., *A guide to first-passage processes*. Cambridge University Press: Cambridge, **2001**.
27. Wu, K. F.; Rodriguez-Cordoba, W. E.; Liu, Z.; Zhu, H. M.; Lian, T. Q., Beyond band alignment: Hole localization driven formation of three spatially separated long-lived exciton states in CdSe/CdS nanorods. *ACS Nano,* **2013,** *7*, 7173-7185.
28. Wu, K.; Rodriguez-Cordoba, W.; Lian, T., Exciton localization and dissociation dynamics in CdS and CdS-Pt quantum confined nanorods: Effect of nonuniform rod diameters. *J. Phys. Chem. B,* **2014,** *118*, 14062-14069.
29. Rudin, S.; Reinecke, T. L.; Segall, B., Temperature-dependent exciton linewidths in semiconductors. *Phys. Rev. B,* **1990,** *42*, 11218-11231.
30. Mack, T. G.; Jethi, L.; Kambhampati, P., Temperature dependence of emission line widths from semiconductor nanocrystals reveals vibronic contributions to line broadening processes. *J. Phys. Chem. C,* **2017,** *121*, 28537-28545.
31. Grimaldi, G.; Geuchies, J. J.; van der Stam, W.; du Fossé, I.; Brynjarsson, B.; Kirkwood, N.; Kinge, S.; Siebbeles, L. D. A.; Houtepen, A. J., Spectroscopic evidence for the contribution of holes to the bleach of Cd-chalcogenide quantum dots. *Nano Lett.,* **2019**, DOI: 10.1021/acs.nanolett.9b00164.
32. Reid, K. R.; McBride, J. R.; La Croix, A. D.; Freymeyer, N. J.; Click, S. M.; Macdonald, J. E.; Rosenthal, S. J., Role of surface morphology on exciton recombination in single quantum dot-in-rods revealed by optical and atomic structure correlation. *ACS Nano,* **2018,** *12*, 11434-11445.
33. Utterback, J. K.; Wilker, M. B.; Mulder, D. W.; King, P. W.; Eaves, J. D.; Dukovic, G., Quantum efficiency of charge transfer competing against nonexponential processes: The case of electron transfer from CdS nanorods to hydrogenase. *J. Phys. Chem. C,* **2019,** *123*, 886-896.
34. Marchioro, A.; Whitham, P. J.; Knowles, K. E.; Kilburn, T. B.; Reid, P. J.; Gamelin, D. R., Tunneling in the delayed luminescence of colloidal CdSe, Cu^{+}-doped CdSe, and $CuInS_2$ semiconductor nanocrystals and relationship to blinking. *J. Phys. Chem. C,* **2016,** *120*, 27040-27049.
35. Whitham, P. J.; Knowles, K. E.; Reid, P. J.; Gamelin, D. R., Photoluminescence blinking and reversible electron trapping in copper-doped CdSe nanocrystals. *Nano Lett.,* **2015,** *15*, 4045-4051.
36. Tsui, E. Y.; Carroll, G. M.; Miller, B.; Marchioro, A.; Gamelin, D. R., Extremely slow spontaneous electron trapping in photodoped n-type CdSe nanocrystals. *Chem. Mater.,* **2017,** *29*, 3754-3762.

37. Chestnoy, N.; Harris, T. D.; Hull, R.; Brus, L. E., Luminescence and photophysics of CdS semiconductor clusters - the nature of the emitting electronic state. *J. Phys. Chem.,* **1986,** *90*, 3393-3399.
38. Baker, D. R.; Kamat, P. V., Tuning the emission of CdSe quantum dots by controlled trap enhancement. *Langmuir,* **2010,** *26*, 11272-11276.
39. Madelung, O., *Semiconductors—Basic Data*. 2nd ed.; Springer: Berlin, **1996**.
40. Marcus, R. A.; Sutin, N., Electron transfers in chemistry and biology. *Biochim. Biophys. Acta,* **1985,** *811*, 265-322.
41. Deskins, N. A.; Dupuis, M., Electron transport via polaron hopping in bulk TiO_2: A density functional theory characterization. *Phys. Rev. B,* **2007,** *75*, 195212.
42. Alexandrov, A. S.; Mott, S. N., *Polarons & Bipolarons*. World Scientific: Singapore, **1995**.
43. Jortner, J., Temperature-dependent activation-energy for electron-transfer between biological molecules. *J. Chem. Phys.,* **1976,** *64*, 4860-4867.
44. Beecher, A. N.; Dziatko, R. A.; Steigerwald, M. L.; Owen, J. S.; Crowther, A. C., Transition from molecular vibrations to phonons in atomically precise cadmium selenide quantum dots. *J. Am. Chem. Soc.,* **2016,** *138*, 16754-16763.
45. Klimov, V. I., Spectral and dynamical properties of multilexcitons in semiconductor nanocrystals. *Annu. Rev. Phys. Chem.,* **2007,** *58*, 635-673.
46. Press, W. H.; Teukolsky, S. A.; Vetterling, W. T.; Flannery, B. P., *Numerical Recipes: The Art of Scientific Computing*. 3rd ed.; Cambridge University Press: Cambridge, **2007**.

SUPPORTING INFORMATION
for

Temperature-Dependent Transient Absorption Spectroscopy Elucidates Trapped-Hole Dynamics in CdS and CdSe Nanorods

James K. Utterback, Jesse L. Ruzicka, Hayden Hamby, Joel D. Eaves, Gordana Dukovic*

Department of Chemistry, University of Colorado Boulder, Boulder, Colorado 80309, USA

*Correspondence to: gordana.dukovic@colorado.edu

Table of Contents

I. Experimental

Synthesis and purification of CdS nanorods (NRs)

Nonuniform CdS NRs were synthesized following established synthetic methods.[1] The CdS seeds were synthesized from a starting mixture containing 0.108 g cadmium oxide (CdO, 99.99% Aldrich), 0.604 g octadecylphosphonic acid (ODPA, 99%, PCI Synthesis), and 3.300 g trioctylphosphine oxide (TOPO, 99%, Aldrich). After heating to 320ºC, a stock solution of the sulfur precursor (0.172 g hexamethyldisilathiane ($(TMS)_2S$, synthesis grade, Aldrich) in 3 g of tributylphosphine (TBP, 97%, Aldrich)) was quickly injected. Nanocrystal growth proceeded for 3 min at 250ºC. The reaction was stopped by removing the heating mantle and injecting 10 mL of a 1:1 (v/v) mixture of anhydrous methanol (99.8%, Sigma-Aldrich) and anhydrous toluene (99.8%, Sigma-Aldrich). The CdS seeds were then dissolved in a minimal amount of anhydrous toluene, precipitated with methanol to wash away unreacted precursor, and the final product was dissolved in trioctylphosphine (TOP, 97%, Strem). The purified CdS seeds had their lowest-energy exciton peak at 399 nm. The NRs were synthesized from a starting solution of 0.086 g CdO, 3 g TOPO, 0.292 g ODPA, and 0.084 g hexylphosphonic acid (HPA, 99%, PCI Synthesis). The solution was heated to 350ºC followed by injection of 1.5 g of TOP. When the temperature of the Cd-containing solution stabilized at 350°C, the solution containing both CdS seeds and sulfur precursor—0.120 g of sulfur (S, 99.998%, Aldrich) in 1.5 g of TOP mixed with 8×10^{-8} mol CdS QD seeds—was quickly injected. Nanocrystal growth proceeded for 8 min, after which the solution was cooled and the particles were precipitated and purified with a 1:1:1 acetone/toluene/methanol mixture. After purification, the NRs were size-selected through a precipitation process by slowly increasing the polarity of a nanocrystal-toluene solution with isopropanol.

Synthesis and purification of CdSe NRs

The synthesis for nonuniform CdSe NRs was adapted from a previously reported procedure.[2] The synthesis of the batch of CdSe NRs used in the experiments presented here was described in detail previously.[3]

Ligand exchange

The hydrophobic native surface-capping ligands of both the as-synthesized CdS and CdSe NRs were replaced with 3-mercaptoproponate (3-MPA) ligands following a previously reported procedure,[4] and the resulting particles were redispersed in anhydrous methanol.

UV-visible absorption spectroscopy

The samples used for UV-visible absorption contained CdS NRs or CdSe NRs capped with 3-MPA ligands, dispersed in 4:1 ethanol:methanol (v/v), and were sealed under Ar in a 1 cm × 1 cm quartz cuvette. UV-visible absorption spectra were recorded using an Agilent 8453 spectrophotometer equipped with tungsten and deuterium lamps.

Transmission electron microscopy

Transmission electron micrograph (TEM) samples were prepared by drop-casting CdS and CdSe NRs with native ligands onto TEM grids (300 mesh copper grids with carbon film, Electron Microscopy Science). TEM images in Figure S1 were collected on a FEI Tecnai Spirit BioTwin operating at 120 kV. The dimensions of the NRs were determined by measuring more than 200 particles in TEM using ImageJ software.[5] High-resolution TEM images (Figure 1) were collected on a FEI Tecnai ST20 operating at 200 kV.

Transient absorption (*TA*) *spectroscopy*

The complete experimental set-up used for TA experiments here has been described previously.[6] Briefly, femtosecond TA spectroscopy measurements in the 100 fs–to–3 ns time window were performed using a regeneratively amplified Ti:sapphire laser (Solstice, Spectra-Physics, 800 nm, 100 fs, 1 kHz, 3.5 mJ/pulse), an optical parametric amplifier (TOPAS-C, Light Conversion), and a HELIOS spectrometer (Ultrafast Systems, LLC) with the white-light continuum being generated from the 800 nm Solstice output using a sapphire plate. Nanosecond TA spectroscopy (0.3 ns to 400 μs) was performed using an EOS spectrometer (Ultrafast Systems, LLC) where the white-light probe beam (400–900 nm, 0.3 ns, 2 kHz) was generated by a Nd:YAG laser focused into a photonic crystal fiber and the pump-probe delay was controlled by an electronic delay generator (CNT-90, Pendulum Instruments). The pump and probe beams were focused and overlapped on the sample, and the probe beam was split into probe and reference detection channels.

Temperature dependence studies were carried out using a Janis STVP-100 continuous flow optical cryostat with quartz windows equipped with a home-built 1 cm cuvette holder. The samples were held in a 1 cm cryogenic cuvette from FireflySci (type 66FL) equipped with a screw cap. The cuvette was cooled under flowing nitrogen vapor and the temperature was controlled with a LakeShore 335 temperature controller connected to two thermocouple/heating element pairs, one at the head of the sample holder and the other in the vaporizer assembly located at the bottom of the cryostat.

II. Transmission electron microscopy images

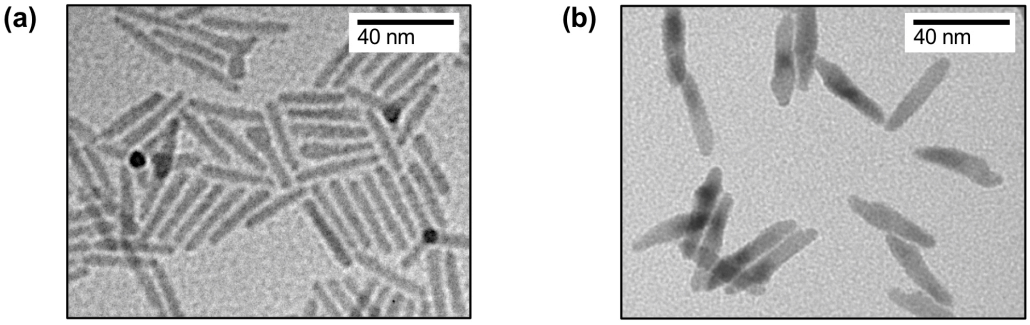

Figure S1. Transmission electron microscopy images of (a) CdS and (b) CdSe NRs. In the samples of NRs studied here, many NRs are nonuniform in diameter.

III. Temperature dependence of the TA bleach peak of CdS and CdSe nanorods

Figure S2 shows the centers and widths of the main bleach peak of CdS and CdSe NRs from Figure 2 as a function of temperature. The peak shifting in Figure S2a was fit to a line, giving $-\partial E_{\mathrm{max}}/\partial T$ values of $(3.6 \pm 0.2) \times 10^{-4}$ eV/K and $(2.4 \pm 0.2) \times 10^{-4}$ eV/K for CdS and CdSe NRs, respectively. These values are consistent with previous reports for bulk and nanocrystalline CdS and CdSe.[7] The width of the main bleach feature in Figure S2b, measured as the full width at half maximum (FWHM), was fit to a previously described model:[8] $\Gamma(T) = \Gamma_{\mathrm{inh}} + \sigma T + \Gamma_{\mathrm{LO}}\left(e^{-E_{\mathrm{LO}}/k_{\mathrm{B}}T} - 1\right)^{-1}$, where $\Gamma(T)$ is the temperature-dependent linewidth, Γ_{inh} is the temperature-independent inhomogeneous linewidth, σ is the exciton–acoustic phonon coupling coefficient, Γ_{LO} is the band-edge exciton–LO phonon coupling coefficient, E_{LO} is the LO phonon energy, k_{B} is the Boltzmann constant, and T is the temperature. Fits were performed using known values of σ = 0.2 μeV/K and E_{LO} = 36.8 meV for CdS NRs,[8-10] and σ = 8 μeV/K and E_{LO} = 26.1 meV for CdSe NRs,[8,11-13] giving Γ_{inh} = 28 ± 1 meV and Γ_{LO} = 51 ± 2 meV for CdS NRs, and Γ_{inh} = 58 ± 4 and Γ_{LO} = 65 ± 9 meV for CdSe NRs. These values of Γ_{inh} are consistent with the polydispersity of each sample and the values of Γ_{LO} are consistent with previous reports for bulk and nanocrystalline CdS and CdSe.[8] This analysis shows that the changes in the peak centers and widths of the main TA bleach peak with temperature are quantitatively consistent with expected trends for CdS and CdSe nanocrystals. This spectral shifting with temperature was accounted for when spectral averaging was performed in order to isolate rod and bulb decay traces (see Methods).

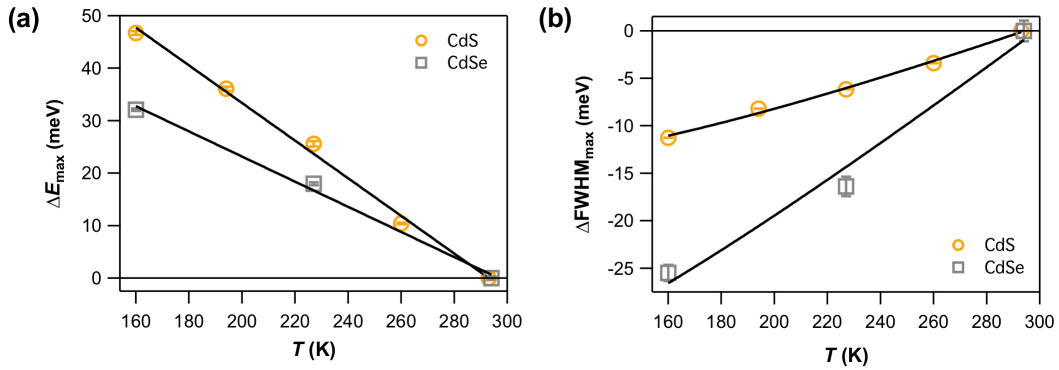

Figure S2. Characterization of the main TA bleach peak as a function of temperature for CdS and CdSe NRs, measured 100–300 ns and 1–3 ns after excitation, respectively. (a) Bleach peak shift, ΔE_{max}, relative to 294 K. At 294 K, E_{max} is 2.7112 and 1.8848 eV for CdS and CdSe NRs, respectively. (b) Bleach peak width, $\Delta\mathrm{FWHM}_{\mathrm{max}}$, relative to 294 K. At 294 K, $\mathrm{FWHM}_{\mathrm{max}}$ is 43 and 97 meV for CdS and CdSe NRs, respectively.

IV. Temperature dependence of charge separation in nonuniform CdS and CdSe nanorods

Figure S3 demonstrates rod-to-bulb electron population transfer in nonuniform CdS and CdSe NRs. In all experiments presented here, the CdS and CdSe NRs were excited above the band gap, which primarily excite the rods rather than the bulbs because they comprise a larger volume fraction of the nanostructures.[3,14-17] Driven by the lower confinement energy of the bulb state compared to the rod state in nonuniform NRs, photoexcited electrons that are initially generated in the rod morphological feature transfer to the bulb. As has been demonstrated before in room temperature TA studies,[3,15,17,18] this process manifests as a partial decay of the rod signal (Figure S3a,b) and a corresponding rise of the bulb signal (Figure S3c,d). Here we find that, in CdS NRs, the TA time traces overlap within the noise at each temperature studied, indicating that the kinetics of rod-to-bulb electron localization do not depend strongly on temperature over the 160–294 K range. At all temperatures, rod-to-bulb electron localization constitutes ~25% of the decay and is complete after a few hundred picoseconds in CdS NRs. In CdSe NRs the extent of electron localization depends on the temperature, reaching 68%, 73% and 100% at 294, 227 and 160 K, respectively. Localization is complete after a few hundred picoseconds at each temperature. Hole trapping in CdS and CdSe nanocrystals is fast in comparison, occurring on a sub-picosecond timescale.[3,19-28] These observations suggest that spatial separation between the electron localized in the bulb and the hole trapped on the rod occurs at each temperature studied.

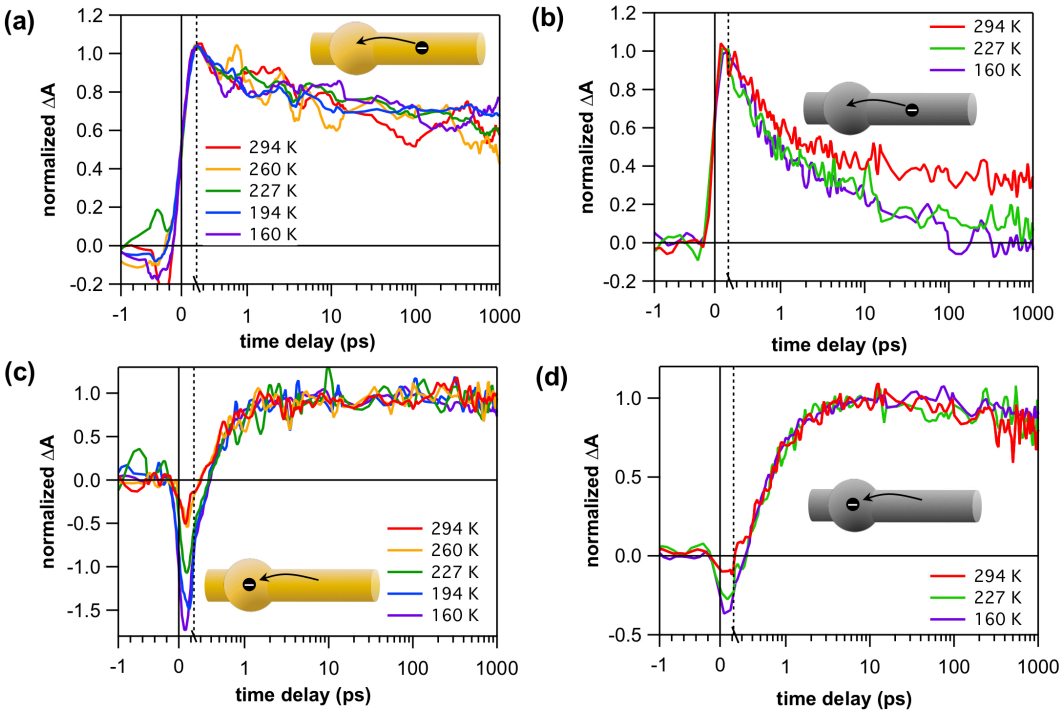

Figure S3. Rod-to-bulb electron localization in CdS and CdSe NRs for temperatures in the range of 160 to 294 K. Formation and partial decay of rod signal in (a) CdS NRs after 400 nm excitation and (b) CdSe NRs after 600 nm excitation, and corresponding rise of bulb signal in (c) CdS NRs and (d) CdSe NRs, collected at indicated temperatures. Time traces for isolated rod and bulb signals were obtained by averaging traces at the wavelengths reported in the Methods section of the manuscript. All traces are normalized to have maximum amplitudes of 1. The time axes are linear for the first 0.25 ps and logarithmic thereafter.

V. Temperature dependence of electron relaxation in uniform CdS nanorods

The rod signal remaining after electron localization is complete is due to uniform NRs in the sample.[3,17] The TA decay traces that correspond to electron dynamics in uniform CdS NRs after the timescale of rod-to-bulb electron localization at different temperatures are shown below. These decay traces are due to uniform NRs in solution. In contrast to the power-law recombination dynamics of spatially separated electrons and trapped holes in nonuniform NRs (Figure 2), spatially overlapping electrons and trapped holes in uniform NRs exhibit exponential asymptotic decay at all temperatures. The timescale of the exponential tail, which is likely due to recombination, increases as temperature decreases. Additionally, as the temperature is reduced, a broad, non-exponential, pre-asymptotic decay component emerges that precedes the exponential cutoff, similar to the pre-asymptotic decay of nonuniform NRs (Figure 2 and S5). The existence of this behavior in both uniform and nonuniform NRs suggests a common mechanism that is unrelated to trapped-hole diffusion, such as electron trapping with a distribution in trapping rates. Nonetheless, the asymptotic exponential tail in uniform NRs and the power-law tail in nonuniform NRs are easily distinguished from this pre-asymptotic decay component.

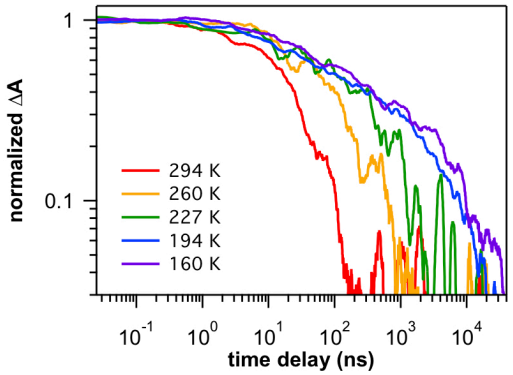

Figure S4. TA time traces of rod signal in uniform CdS NRs over 160–294 K. Time traces for the isolated rod signals at each temperature were obtained by averaging traces at the wavelengths reported in the Methods section of the manuscript.

We do not have data analogous to Figure S4 for CdSe NRs because the extent of electron localization is high (Figure S3b) and there are few uniform NRs in the sample.

VI. Upper and lower bounds for hole-hopping rate

Here we describe how we obtained upper and lower bounds for the hole-hopping rate presented in the manuscript. The pre-asymptotic decay of the charge-separated state in Figure 2 depends on temperature. As the temperature decreases, the entrance into the power-law occurs at progressively longer times. For times after rod-to-bulb electron localization we assume a form for the bulb electron survival probability, $S(t)$, that comes from one-dimensional diffusion–annihilation where all trapped holes start at the same distance from the bulb, z_0, and diffuse with diffusion coefficient D. This is a reasonable approximation because for long times $S(t)$ will be insensitive to the shape of the distribution of the initial positions and depends only on the mean, z_0.[17] In this regime,

$$S(t) = \mathrm{erf}\left(\sqrt{\tau/t}\right), \tag{S1}$$

where the $\tau = z_0^2/4D$.[17,29] Expanding $S(t)$ asymptotically for long times yields the power law: $S(t) \propto t^{-1/2}$. Because the onset of the power-law tail occurs for all times $t > \tau$ in eq S1, we take the upper bound for τ to be the time at which the power-law tail begins (Figure S5a), defined as the time at which relative difference between a fit to a $t^{-1/2}$ power-law tail and the data reached 5%. Separately, we obtained the lower bound for τ by matching eq S1 to the initial decay as well as the power-law tail (Figure S5a). This gives the smallest possible value for τ because any smaller value would underestimate the amplitude of the signal at late times; τ cannot be any smaller because additional decay components would act to reduce the amplitude at late times even further. These definitions for the upper and lower bounds of τ are illustrated using CdS NRs at 260 K as an example in Figure S5a, and the fits to every CdS and CdSe NR trace are shown in Figures S5b,c.

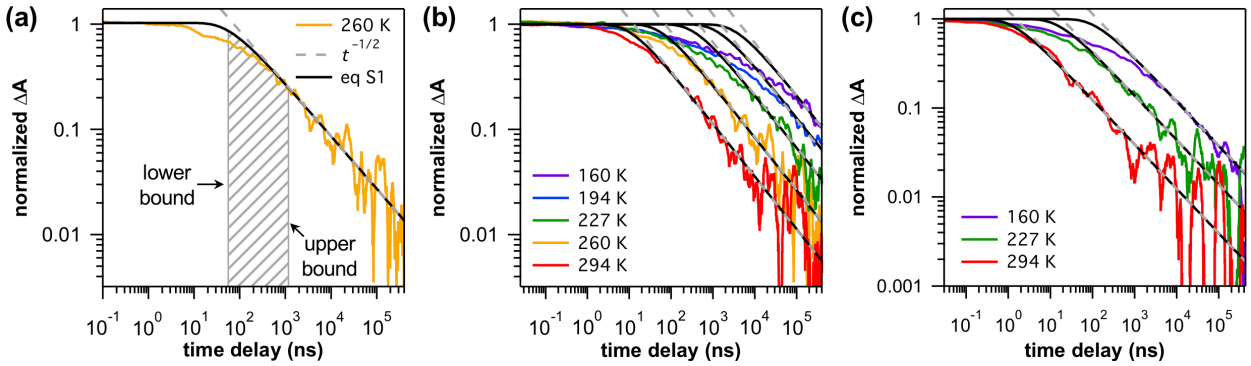

Figure S5. Obtaining upper and lower bounds of τ for CdS and CdSe NRs as a function of temperature. (a) Illustrative example of obtaining upper and lower bounds of τ for CdS NRs at 260 K. The upper bound is the onset of the power-law tail while the lower bound is found by fitting the beginning and tail of the decay trace to eq S1. The shaded region represents the range of possible τ values. (b) Fits of eq S1 and the power-law tail for CdS NRs at the indicated temperatures. (c) Fits of eq S1 and the power-law tail for CdSe NRs at the indicated temperatures.

VII. Absorption spectra of CdS and CdSe nanorods

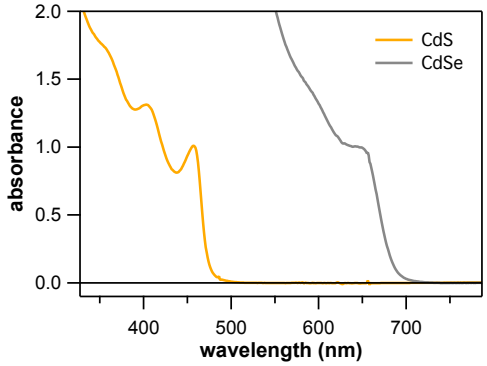

Figure S6. Room-temperature UV-visible absorption spectra of CdS and CdSe NRs in 4:1 ethanol:methanol (v/v).

VIII. References

1. Carbone, L.; Nobile, C.; De Giorgi, M.; Sala, F. D.; Morello, G.; Pompa, P.; Hytch, M.; Snoeck, E.; Fiore, A.; Franchini, I. R., et al., Synthesis and micrometer-scale assembly of colloidal CdSe/CdS nanorods prepared by a seeded growth approach. *Nano Lett.,* **2007,** *7*, 2942-2950.
2. Lee, D.; Kim, W. D.; Lee, S.; Bae, W. K.; Lee, S.; Lee, D. C., Direct Cd-to-Pb exchange of CdSe nanorods into PbSe/CdSe axial heterojunction nanorods. *Chem. Mater.,* **2015,** *27*, 5295-5304.
3. Utterback, J. K.; Hamby, H.; Pearce, O.; Eaves, J. D.; Dukovic, G., Trapped-hole diffusion in photoexcited CdSe nanorods. *J. Phys. Chem. C,* **2018,** *122*, 16974-16982.
4. Brown, K. A.; Wilker, M. B.; Boehm, M.; Dukovic, G.; King, P. W., Characterization of photochemical processes for H_2 production by CdS nanorod-[FeFe] hydrogenase complexes. *J. Am. Chem. Soc.,* **2012,** *134*, 5627-5636.
5. Schneider, C. A.; Rasband, W. S.; Eliceiri, K. W., NIH Image to ImageJ: 25 years of image analysis. *Nat. Methods,* **2012,** *9*, 671-675.
6. Tseng, H. W.; Wilker, M. B.; Damrauer, N. H.; Dukovic, G., Charge transfer dynamics between photoexcited CdS nanorods and mononuclear Ru water-oxidation catalysts. *J. Am. Chem. Soc.,* **2013,** *135*, 3383-3386.
7. Madelung, O., *Semiconductors—Basic Data*. 2nd ed.; Springer: Berlin, 1996.
8. Rudin, S.; Reinecke, T. L.; Segall, B., Temperature-dependent exciton linewidths in semiconductors. *Phys. Rev. B,* **1990,** *42*, 11218-11231.
9. Shiang, J. J.; Risbud, S. H.; Alivisatos, A. P., Resonance Raman studies of the ground and lowest electronic excited-state in CdS nanocrystals. *J. Chem. Phys.,* **1993,** *98*, 8432-8442.
10. Kulik, D.; Htoon, H.; Shih, C. K.; Li, Y. D., Photoluminescence properties of single CdS nanorods. *J. Appl. Phys.,* **2004,** *95*, 1056-1063.
11. Gindele, F.; Hild, K.; Langbein, W.; Woggon, U., Temperature-dependent line widths of single excitons and biexcitons. *J. Lumin.,* **2000,** *87-9*, 381-383.
12. Lange, H.; Artemyev, M.; Woggon, U.; Thomsen, C., Geometry dependence of the phonon modes in CdSe nanorods. *Nanotechnology,* **2009,** *20*, 045705.
13. Beecher, A. N.; Dziatko, R. A.; Steigerwald, M. L.; Owen, J. S.; Crowther, A. C., Transition from molecular vibrations to phonons in atomically precise cadmium selenide quantum dots. *J. Am. Chem. Soc.,* **2016,** *138*, 16754-16763.

14. Yu, W. W.; Qu, L.; Guo, W.; Peng, X., Experimental determination of the extinction coefficient of CdTe, CdSe, and CdS nanocrystals. *Chem. Mater.,* **2003,** *15*, 2854-2860.
15. Wu, K. F.; Rodriguez-Cordoba, W. E.; Liu, Z.; Zhu, H. M.; Lian, T. Q., Beyond band alignment: Hole localization driven formation of three spatially separated long-lived exciton states in CdSe/CdS nanorods. *ACS Nano,* **2013,** *7*, 7173-7185.
16. Yang, Y.; Wu, K. F.; Chen, Z. Y.; Jeong, B. S.; Lian, T. Q., Competition of branch-to-core exciton localization and interfacial electron transfer in CdSe tetrapods. *Chem. Phys.,* **2016,** *471*, 32-38.
17. Utterback, J. K.; Grennell, A. N.; Wilker, M. B.; Pearce, O.; Eaves, J. D.; Dukovic, G., Observation of trapped-hole diffusion on the surfaces of CdS nanorods. *Nat. Chem.,* **2016,** *8*, 1061-1066.
18. Wu, K.; Rodriguez-Cordoba, W.; Lian, T., Exciton localization and dissociation dynamics in CdS and CdS-Pt quantum confined nanorods: Effect of nonuniform rod diameters. *J. Phys. Chem. B,* **2014,** *118*, 14062-14069.
19. Klimov, V.; Bolivar, P. H.; Kurz, H., Ultrafast carrier dynamics in semiconductor quantum dots. *Phys. Rev. B,* **1996,** *53*, 1463-1467.
20. Klimov, V. I.; Schwarz, C. J.; McBranch, D. W.; Leatherdale, C. A.; Bawendi, M. G., Ultrafast dynamics of inter- and intraband transitions in semiconductor nanocrystals: Implications for quantum-dot lasers. *Phys. Rev. B,* **1999,** *60*, R2177-R2180.
21. Underwood, D. F.; Kippeny, T.; Rosenthal, S. J., Ultrafast carrier dynamics in CdSe nanocrystals determined by femtosecond fluorescence upconversion spectroscopy. *J. Phys. Chem. B,* **2001,** *105*, 436-443.
22. Burda, C.; Link, S.; Mohamed, M.; El-Sayed, M., The relaxation pathways of CdSe nanoparticles monitored with femtosecond time-resolution from the visible to the IR: Assignment of the transient features by carrier quenching. *J. Phys. Chem. B,* **2001,** *105*, 12286-12292.
23. McArthur, E. A.; Morris-Cohen, A. J.; Knowles, K. E.; Weiss, E. A., Charge carrier resolved relaxation of the first excitonic state in CdSe quantum dots probed with near-infrared transient absorption spectroscopy. *J. Phys. Chem. B,* **2010,** *114*, 14514-14520.
24. Knowles, K. E.; McArthur, E. A.; Weiss, E. A., A multi-timescale map of radiative and nonradiative decay pathways for excitons in CdSe quantum dots. *ACS Nano,* **2011,** *5*, 2026-2035.
25. Wu, K. F.; Zhu, H. M.; Liu, Z.; Rodriguez-Cordoba, W.; Lian, T. Q., Ultrafast charge separation and long-lived charge separated state in photocatalytic CdS-Pt nanorod heterostructures. *J. Am. Chem. Soc.,* **2012,** *134*, 10337-10340.
26. Keene, J. D.; McBride, J. R.; Orfield, N. J.; Rosenthal, S. J., Elimination of hole-surface overlap in graded CdS_xSe_{1-x} nanocrystals revealed by ultrafast fluorescence upconversion spectroscopy. *ACS Nano,* **2014,** *8*, 10665-10673.
27. Li, X.; Feng, D. H.; Tong, H. F.; Jia, T. Q.; Deng, L.; Sun, Z. R.; Xu, Z. Z., Hole surface trapping dynamics directly monitored by electron spin manipulation in CdS nanocrystals. *J. Phys. Chem. Lett.,* **2014,** *5*, 4310-4316.
28. Utterback, J. K.; Wilker, M. B.; Mulder, D. W.; King, P. W.; Eaves, J. D.; Dukovic, G., Quantum efficiency of charge transfer competing against nonexponential processes: The case of electron transfer from CdS nanorods to hydrogenase. *J. Phys. Chem. C,* **2019,** *123*, 886-896.
29. Redner, S., *A guide to first-passage processes*. Cambridge University Press: Cambridge, **2001**.